J Math Imaging Vis (2018) 60:1–17
https://doi.org/10.1007/s10851-017-0735-3

Image Segmentation with Depth Information via Simplified Variational Level Set Formulation

Lu Tan[1] · Zhenkuan Pan[1] · Wanquan Liu[3] · Jinming Duan[2] · Weibo Wei[1] · Guodong Wang[1]

Received: 1 December 2016 / Accepted: 27 April 2017 / Published online: 13 May 2017

Abstract Image segmentation with depth information can be modeled as a minimization problem with Nitzberg–Mumford–Shiota functional, which can be transformed into a tractable variational level set formulation. However, such formulation leads to a series of complicated high-order nonlinear partial differential equations which are difficult to solve efficiently. In this paper, we first propose an equivalently reduced variational level set formulation without using curvatures by taking level set functions as signed distance functions. Then, an alternating direction method of multipliers (ADMM) based on this simplified variational level set formulation is designed by introducing some auxiliary variables, Lagrange multipliers via using alternating optimization strategy. With the proposed ADMM method, the minimization problem for this simplified variational level set formulation is transformed into a series of sub-problems, which can be solved easily via using the Gauss–Seidel iterations, fast Fourier transform and soft thresholding formulas. The level set functions are treated as signed distance functions during computation process via implementing a simple algebraic projection method, which avoids the traditional re-initialization process for conventional variational level set methods. Extensive experiments have been conducted on both synthetic and real images, which validate the proposed approach, and show advantages of the proposed ADMM projection over algorithms based on traditional gradient descent method in terms of computational efficiency.

Keywords Segmentation with depth · Nitzberg–Mumford–Shiota (NMS)functional · Variational level set formulation · Alternating direction method of multipliers (ADMM) · Projection method · Fast Fourier Transform (FFT) · Soft thresholding formulas

1 Introduction

The segmentation with depth information is a 2.1D sketch problem [1–3] in computer vision. Its goal is to reconstruct the complete shapes of occluded objects and their ordering relation in a specific scene based on only one single image via using segmentation techniques. Such segmentation plays an important role in image analysis and computer vision, such as object recognition and tracking. It is also a fundamental preprocessing step to some more complicated problems such as illusory shape recovery [4,5].

In early 1990s, Nitzberg et al. [6] innovatively modeled the segmentation with depth as a minimization problem for an energy functional, which is called the NMS model. This model combines the classical Mumford–Shah model [7] for variational image segmentation and Euler's elastica terms [8]. In order to optimize the NMS model in a tractable manner, authors in [6] have decomposed such problem into three successive steps: finding the edges and T-junctions in the image; hypothesizing the ordering relation of objects to be segmented and obtaining the associated minimum of energy functional; determining the objects' ordering and the reconstructed shapes according to the minimum functional in the second step. This NMS model is a

✉ Wanquan Liu
w.liu@curtin.edu.au

[1] College of Information Engineering, Qingdao University, Qingdao, China

[2] School of Computer Science, University of Nottingham, Nottingham, UK

[3] Department of Computing, Curtin University, Bentley, Perth, Australia

foundation for this type of segmentation problems associated with depth information, and many possible solutions have been proposed based on this model as described below.

Instead of the tedious multiple step procedure aforementioned, Esedoglu and March [9] transformed the original NMS model into an equivalent one based on Γ-convergence concept [10,11] and its aim is to approximate the terms associated with length and elastica. Such derived model was claimed and demonstrated to be more tractable without requirement of T-junctions detection. For the computational efficiency, they designed a fast scheme by combing the semi-implicit discretization and fast Fourier transform (FFT) methods. But due to the over simplification of curvature-related terms in quadratic form, their model cannot preserve the corners of the recovered shapes, as they pointed out in [9].

Another rigorous approximation for the NMS model is based on variational level set method [13–16], which was proposed by Zhu et al. [12]. By making use of the standard variational method, they have derived a series of higher-order evolution equations including level set functions and then proposed the Smereka's semi-implicit method [17] with FFT solver. However, it is difficult to discretize the fourth-order nonlinear partial differential equations (PDEs) in their approach. Additionally, they did not consider the definition of level set functions as signed distance functions during computation process as did in [12].

Recently, another similar work was conducted by Zhu et al. [18], where they proposed the Chan–Vese–Euler model by combining the Chan–Vese model and Euler elastica regularizer with an aim to recover the missed parts of contours. In order to minimize the proposed model efficiently, they designed a fast alternating direction method of multipliers (ADMM) [19,20]. Although this model can integrate the missing parts to form a complete meaningful object, it was designed only for one foreground shape recovery problem without considering segmentation with depth information. Moreover, their work was based on binary label function method [22] or piecewise constant level set function method [21].

The curvature-related terms play crucial roles in the NMS model, but they also brought computational complexity due to the nonlinear higher-order derivatives. This issue also appears in other variational models of imaging sciences on the non-texture image inpainting [23,24], illusory contours reconstruction [4,5], image denoising [25–28] with feature (edge, corner, smoothness, contrast, etc.) preserving. In order to improve the computational efficiency and avoid solving nonlinear higher-order PDEs, some fast ADMM methods are systematically investigated in [27–30] for energy minimization problems associated with curvature terms.

Motivated by works in [27–30], in this paper, we focus on developing a fast ADMM method for optimizing the NMS model [6], which can be rewritten as a variational level set formulation [12]. The main difference between the variational level set formulation and the models in [23–30] is that the variational level set formulation in this paper is constrained by some nonlinear Eikonal equations of level set functions based on definition of signed distance functions. Usually, these constrained equations are guaranteed to be satisfied by solving a dynamic Hamilton–Jacobi equation using the upwind finite difference scheme [31], fast sweeping method [32], or they can be coped with penalty function method [33,34] to get rid of these constraints.

The ADMM-projection (ADMM-P is used for abbreviation in the following parts of this paper) method proposed in this paper is based on the simplified variational level set formulation by replacing curvatures with Laplacians of level set functions on the premise that the Eikonal equations are satisfied during computation process. Another salient feature of this method is that the Eikonal equations can be satisfied indirectly by means of introducing auxiliary variables and implementing a direct projection [35,36], which are suitable for the simplified variational level set formulation.

The paper is organized as follows: in Sect. 2, the variational level set formulation of the NMS functional along with its traditional gradient descent method (GDM is used for abbreviation in the follows) is reviewed; in Sect. 3, we derive the simplified variational level set formulation as an equivalent one of the NMS, and then design a fast ADMM-P method for the simplified variational level set formulation by transforming it into some sub-minimization problems for efficient computation in Sect. 4; in Sect. 5, extensive numerical experiments on different type images are conducted to illustrate the efficiency of the proposed model and its ADMM-P method. Concluding remarks are presented in Sect. 6.

2 The Variational Level Set Formulation for the NMS Model and its GDM Method

In this section, we will review the variational level set formulation of the NMS model first and then highlight our contributions clearly in Sects. 3 and 4. In [6], Nitzberg et al. defined the problem of segmentation with depth information as a problem of recovering occluded shapes and their ordering relations based on a 2D image. This problem is investigated with the following three assumptions: (1) there is no self-occlusion on the surface of each object; (2) the objects are not entangled with each other; (3) the pixel intensities of each object are approximately constant and different from each other. The variables defined in this problem are in three folds: the shapes of the regions $R_1, R_2, \ldots, R_n$ to

which different objects belong; the ordering relations among objects; the pixel intensities of objects.

Without loss of generality, one can assume that the objects $R_1, R_2, \ldots, R_n$ in an image are in ascending order, i. e., R_1 is the nearest object to the observer while R_n is the farthest one (i. e. background). Let R_i' be defined as the visible part of R_i, i.e., $R_1' = R_1$, $R_i' = R_i - \bigcup_{j<i} R_j$, $(i = 2, \ldots, n)$. In addition, $R_{n+1}' = \Omega - \bigcup_{j<n+1} R_j$ is defined as the visible background. Based on the above assumptions and definitions, the NMS functional is formulated as in [6]

$$E = \sum_{i=1}^{n} \int_{\partial R_i \cap \Omega} [\alpha + \beta\phi(\kappa_i)]\mathrm{d}s + \sum_{i=1}^{n+1} \int_{R_i'} (f(x) - c_i)^2 \mathrm{d}x. \tag{1}$$

where α, β are two positive penalty parameters, s is arc length, and $c_i \in R_i$ are pixel intensities of the ith object, κ denotes the curvature of boundary for region R_i. While one of the main difficulties in minimizing the above NMS functional is to calculate the energy term.

By making use of variational method [13–15] and level set method [16], Zhu and Chan proposed the variational level set formulation in [12] to replace the original NMS model. For such purpose, a level set function representing an interface $\Gamma(t)$ (t represents time) is defined implicitly as the zero level set of a Lipchitz continuous function $\varphi : R^2 \to R$, which in turn can be defined in terms of time t as the following signed distance function for efficient computation,

$$\begin{cases} \varphi(x,t) = d\left(\Gamma(t), x\right), \text{ if } x \text{ is inside } \Gamma(t) \\ \varphi(x,t) = 0, \text{ if } x \text{ is at } \Gamma(t) \\ \varphi(x,t) = -d\left(\Gamma(t), x\right), \text{ if } x \text{ is outside } \Gamma(t) \end{cases}. \tag{2}$$

where $d(\Gamma(t), x)$ denotes the shortest Euclidean distance from x to $\Gamma(t)$, and from which its Eikonal equation is derived as $|\nabla\varphi(x,t)| = 1$.

For an image defined in domain Ω with boundary $\Gamma(t)$, according to the co-area and area formulas in [31], we will have

$$length(\Gamma) = \int_{\Omega} |\nabla H(\varphi)| \,\mathrm{d}x = \int_{\Omega} \delta(\varphi)\, |\nabla\varphi| \mathrm{d}x, \tag{3}$$

$$area(\Omega) = \int_{\Omega} H(\varphi)\mathrm{d}x. \tag{4}$$

where $H(\varphi(x))$ and $\delta(\varphi(x))$ are Heaviside function and Dirac delta function, respectively, with the definitions given below.

$$H(\varphi(x)) = \begin{cases} 1, \text{ if } \varphi(x) \geq 0 \\ 0, \text{ otherwise} \end{cases}, \tag{5}$$

$$\delta(\varphi(x)) = \frac{\partial H(\varphi(x))}{\partial\varphi(x)}. \tag{6}$$

In fact, these kinds of original definitions are difficult to calculate as there exist non-differential functions. In practice, these two functions are often approximated via introducing a small positive parameter ε in (5) and (6) [10,11] by denoting as $H_\varepsilon(\varphi(x))$ and $\delta_\varepsilon(\varphi(x))$. In this way, we can obtain some feasible computing forms of Heaviside function and Dirac delta function in [13–16], given by

$$H_\varepsilon(\varphi) = \frac{1}{2}\left(1 + \frac{2}{\pi}\arctan\left(\frac{\varphi}{\varepsilon}\right)\right), \tag{7}$$

$$\delta_\varepsilon(\varphi) = \frac{1}{\pi}\frac{\varepsilon}{\varepsilon^2 + \varphi^2}. \tag{8}$$

By making use of these level set functions $\varphi_i (i = 1, 2, \ldots, n)$, we can represent objects R_i as $R_i = \{x : H(\varphi_i(x)) = 1\}$, each visible part as $R_i' = R_i - \bigcup_{j<i} R_j$ which is given by $R_i' = \{x : H(\varphi_i) \prod_{j=1}^{i-1} (1 - H(\varphi_j)) = 1\}$, thus the term $\sum_{i=1}^{n+1} \int_{R_i'} (f(x) - c_i)^2 \mathrm{d}x$ in (1) can be rewritten as

$$\sum_{i=1}^{n} \left\{ \int_{\Omega} (f - c_i)^2 H(\varphi_i) \prod_{j=1}^{i-1} \big(1 - H(\varphi_j)\big)\mathrm{d}x \right\} + \int_{\Omega} (f - c_{n+1})^2 \prod_{j=1}^{n} \big(1 - H(\varphi_j)\big)\mathrm{d}x. \tag{9}$$

And more importantly, the curvature κ_i can be represented as $\kappa_i = \nabla \cdot (\frac{\nabla\varphi_i}{|\nabla\varphi_i|})$. Now we choose $\phi(\kappa) = |\kappa|$ as the authors of [12] did with the reason that the NMS model (1) can preserve the object corners when $|\kappa|$ becomes large. Thus, the NMS functional (1) can be reformulated with level set functions as below and our major task is to solve the level set functions φ_i

$$E = \sum_{i=1}^{n} \int_{\Omega} [\alpha + \beta\phi(\kappa_i)]|\nabla\varphi_i|\delta(\varphi_i)\mathrm{d}x + \sum_{i=1}^{n} \left\{ \int_{\Omega} (f - c_i)^2 H(\varphi_i) \prod_{j=1}^{i-1} (1 - H(\varphi_j))\mathrm{d}x \right\} + \int_{\Omega} (f - c_{n+1})^2 \prod_{j=1}^{n} (1 - H(\varphi_j))\mathrm{d}x \tag{10}$$

Now, by using the standard variational method, one can obtain the following GDM equations of level set functions via minimization of functional (10).

$$\frac{\partial \varphi_i}{\partial t} = |\nabla\varphi_i| \nabla \cdot \left[\frac{\nabla\varphi_i}{|\nabla\varphi_i|} \Psi(\kappa_i) - \frac{1}{|\nabla\varphi_i|} \left(\nabla \left(\phi'(\kappa_i) |\nabla\varphi_i| \right) - \left(\frac{\nabla\varphi_i}{|\nabla\varphi_i|} \cdot \nabla(\phi'(\kappa_i) |\nabla\varphi_i|) \right) \frac{\nabla\varphi_i}{|\nabla\varphi_i|} \right) \right] - |\nabla\varphi_i| (f - c_i)^2 \prod_{j=1}^{i-1} \left(1 - H(\varphi_j)\right) + |\nabla\varphi_i| \sum_{s=i+1}^{n+1} \left\{ (f - c_s)^2 H(\varphi_s) \prod_{j=1}^{i-1} \left(1 - H(\varphi_j)\right) \prod_{j=i+1}^{s-1} \left(1 - H(\varphi_j)\right) \right\} \tag{11}$$

where $i = 1, 2, \ldots, n$ denotes the number of objects in the image, and $H(\varphi_{n+1}) = 1$ is introduced only for consistency of description. In fact, (11) is a standard Hamilton–Jacobi equation, which can be solved iteratively using some explicit upwind-alike schemes. However, the convergence of such iteration heavily depends on selected time step size. In order to overcome this problem and improve the computational stability, the authors in [12] employed the Smereka's semi-implicit iteration method [17] to relax the Courant–Friedrichs–Lewy condition. In order to improve the computational efficiency further, they employed the FFT method to solve the discretized equations. But discretization of the nonlinear fourth-order derivatives is tedious and is prone to errors. More seriously, they did not pay attention to the requirement of level set functions as the signed distance functions during computational iteration. In order to overcome these computational problems, we will propose a new ADMM projection approach in this paper.

3 ADMM-P Method for Simplified Variational Level Set Formulation

Instead of solving (10) directly by using the conventional variational method and solving the related GDM equations as mentioned in previous section, in this section, we first transform the original minimization problem into several sub-optimization problems by introducing some auxiliary variables and then solve them using the alternating directional optimization strategy.

First, we propose a simplified model of the original problem by considering the property of level set functions as the signed distance functions. If the level set functions are treated as the signed distance functions during computational process with property $|\nabla\varphi_i| = 1 (i = 1, 2, \ldots n)$, the curvatures in (10) can be replaced by Laplacians of level set functions, and in this case $\kappa_i = \nabla \cdot (\frac{\nabla\varphi_i}{|\nabla\varphi_i|}) = \nabla \cdot (\nabla\varphi_i) = \Delta\varphi_i$ can be reduced to $\kappa_i = \nabla \cdot (\nabla\varphi_i)$. Based on this observation, the NMS functional (10) can be rewritten as the following simplified version

$$E = \sum_{i=1}^{n} \int_\Omega [\alpha + \beta |\nabla \cdot (\nabla\varphi_i)|] \delta(\varphi_i) \, dx + \sum_{i=1}^{n} \left\{ \int_\Omega (f - c_i)^2 H(\varphi_i) \prod_{j=1}^{i-1} \left(1 - H(\varphi_j)\right) dx \right\} + \int_\Omega (f - c_{n+1})^2 \prod_{j=1}^{n} \left(1 - H(\varphi_j)\right) dx \tag{12a}$$

$$\text{s.t. } |\nabla\varphi_i| = 1. \tag{12b}$$

Note that Eqs. (12a) and (12b) are equivalent to the original problem (15). Therefore, some fast ADMM algorithms can be directly applied to (12a) and (12b). For such purpose, some auxiliary variables $\vec{w}_i = [w_{i1}, w_{i2}]^T$ and v_i with property $\vec{w}_i \approx \nabla\varphi_i$, $v_i \approx \nabla \cdot \vec{w}_i$ and the Lagrangian multipliers $\vec{\lambda}_{1i}, \lambda_{2i}$ are introduced. In this case, the constraint $|\nabla\varphi_i| = 1$ will be replaced by $|\vec{w}_i| = 1$, and this substitution can avoid the traditional re-initialization process to satisfy $|\nabla\varphi_i| = 1$ by imposing the compulsory constraint for $\vec{w}_i$. And $|\vec{w}_i| = 1$ then can be guaranteed by implementing a projection method easily. Based this observation, we can transform (12a) and (12b) into the following augmented Lagrangian functional with some explicit constraints.

$$\begin{aligned} &E(c, \varphi, \vec{w}, v, \vec{\lambda}_1, \lambda_2) \\ &= \sum_{i=1}^{n} \int_\Omega [\alpha + \beta |v_i|] \delta(\varphi_i) \, dx + \sum_{i=1}^{n} \int_\Omega \vec{\lambda}_{1i} \cdot (\vec{w}_i - \nabla\varphi_i) dx \\ &+ \frac{\mu_1}{2} \sum_{i=1}^{n} \int_\Omega (\vec{w}_i - \nabla\varphi_i)^2 dx + \sum_{i=1}^{n} \int_\Omega \lambda_{2i} (v_i - \nabla \cdot \vec{w}_i) dx \\ &+ \frac{\mu_2}{2} \sum_{i=1}^{n} \int_\Omega (v_i - \nabla \cdot \vec{w}_i)^2 dx, \\ &+ \sum_{i=1}^{n} \left\{ \int_\Omega (f - c_i)^2 H(\varphi_i) \prod_{j=1}^{i-1} \left(1 - H(\varphi_j)\right) dx \right\} \\ &+ \int_\Omega (f - c_{n+1})^2 \prod_{j=1}^{n} \left(1 - H(\varphi_j)\right) dx \end{aligned} \tag{13a}$$

$$\text{s.t. } |\vec{w}_i| = 1, \quad i = 1, 2, \ldots, n. \tag{13b}$$

where μ_1, μ_2 are positive penalty parameters, and $c = \{c_1 \ c_2 \ \ldots \ c_{n+1}\}$, $\varphi = \{\varphi_1 \ \varphi_2 \ \ldots \ \varphi_n\}$, $\vec{w} = \{\vec{w}_1 \ \vec{w}_2 \ \ldots \ \vec{w}_n\}$, $v = \{v_1 \ v_2 \ \ldots \ v_n\}$, $\vec{\lambda}_1 = \{\vec{\lambda}_{11} \ \vec{\lambda}_{12} \ldots \vec{\lambda}_{1n}\}$, $\lambda_2 = \{\lambda_{21} \ \lambda_{22} \ldots \lambda_{2n}\}$. The approximations for $\vec{w}_i \approx \nabla\varphi_i$ and $v_i \approx \nabla \cdot \vec{w}_i$ can be achieved by

the maximization with respect to $\vec{\lambda}_{1i}$ and λ_{2i} in the energy functional (13.1). Meanwhile, the constraint $|\nabla\varphi_i| = 1$ is replaced by $|\vec{w}_i| = 1$, which can be guaranteed by the projection method directly. It is noteworthy that this constraint can also be guaranteed via penalty function method, in which larger computational expense would be inevitable. Next we will propose a new approach to solve this problem.

The proposed ADMM-P method can be implemented in finite steps with stopping criteria. In each step, we can calculate a sub-problem. Also, the sub-problem of minimization is carried out with respect to one variable while keeping other variables to be fixed temporarily. For the formulations (13a) and (13b), we first initialize the unknown values $c^0, \varphi^0, \vec{w}^0, v^0, \vec{\lambda}_1^0, \lambda_2^0$, and then, we start a procedure of optimization step by step. In each step, the minimization of (13a) and (13b) can be divided into following sub-problems

$$c^{k+1} = \operatorname{Arg}\min_{c}\left\{\varepsilon_0(c) = E\left(c, \varphi^k, \vec{w}^k, v^k, \vec{\lambda}_1^k, \lambda_2^k\right)\right\} \quad (14)$$

$$\varphi^{k+1} = \operatorname{Arg}\min_{\varphi}\left\{\varepsilon_1(\varphi) = E\left(c^{k+1}, \varphi, \vec{w}^k, v^k, \vec{\lambda}_1^k, \lambda_2^k\right)\right\} \quad (15)$$

$$\vec{w}^{k+1} = \operatorname{Arg}\min_{\vec{w}}\left\{\varepsilon_1(\vec{w}) = E\left(c^{k+1}, \varphi^{k+1}, \vec{w}, v^k, \vec{\lambda}_1^k, \lambda_2^k\right)\right\} \quad (16a)$$

$$\text{s.t.} \quad \left|\vec{w}_i^{k+1}\right| = 1, i = 1, 2, \ldots, n \quad (16b)$$

$$v^{k+1} = \operatorname{Arg}\min_{v}\left\{\varepsilon_1(v) = E\left(c^{k+1}, \varphi^{k+1}, \vec{w}^{k+1}, v, \vec{\lambda}_1^k, \lambda_2^k\right)\right\} \quad (17)$$

$$\vec{\lambda}_1^{k+1} = \vec{\lambda}_1^k + \mu_1\left(\vec{w}^{k+1} - \nabla\varphi^{k+1}\right) \quad (18)$$

$$\lambda_2^{k+1} = \lambda_2^k + \mu_2(v^{k+1} - \nabla\cdot\vec{w}^{k+1}) \quad (19)$$

where (18) and (19) are responsible for updating of the Lagrange multipliers. These functionals of the above mentioned sub-problems are given, respectively, below.

$$\varepsilon_0(c) = \sum_{i=1}^{n}\left\{\int_\Omega (f-c_i)^2 H\left(\varphi_i^k\right)\prod_{j=1}^{i-1}\left(1 - H\left(\varphi_j^k\right)\right)\mathrm{d}x\right\} + \int_\Omega (f - c_{n+1})^2\prod_{j=1}^{n}\left(1 - H\left(\varphi_j^k\right)\right)\mathrm{d}x \quad (20)$$

$$\begin{aligned}\varepsilon_1(\varphi) = &\sum_{i=1}^{n}\int_\Omega\left[\alpha + \beta\left|v_i^k\right|\right]\delta(\varphi_i)\,\mathrm{d}x \\ &+ \sum_{i=1}^{n}\int_\Omega \vec{\lambda}_{1i}^k\cdot\left(\vec{w}_i^k - \nabla\varphi_i\right)\mathrm{d}x \\ &+ \frac{\mu_1}{2}\sum_{i=1}^{n}\int_\Omega\left(\vec{w}_i^k - \nabla\varphi_i\right)^2\mathrm{d}x \\ &+ \sum_{i=1}^{n}\left\{\int_\Omega\left(f - c_i^{k+1}\right)^2 H(\varphi_i)\right. \\ &\left.\prod_{j=1}^{i-1}(1 - H(\varphi_j))\mathrm{d}x\right\} \\ &+ \int_\Omega\left(f - c_{n+1}^{k+1}\right)^2\prod_{j=1}^{n}(1 - H(\varphi_j))\mathrm{d}x\end{aligned} \quad (21)$$

$$\begin{aligned}\varepsilon_2(\vec{w}) = &\sum_{i=1}^{n}\int_\Omega \vec{\lambda}_{1i}^k\cdot\left(\vec{w}_i - \nabla\varphi_i^{k+1}\right)\mathrm{d}x \\ &+ \frac{\mu_1}{2}\sum_{i=1}^{n}\int_\Omega\left(\vec{w}_i - \nabla\varphi_i^{k+1}\right)^2\mathrm{d}x \\ &+ \sum_{i=1}^{n}\int_\Omega\lambda_{2i}^k\left(v_i^k - \nabla\cdot\vec{w}_i\right)\mathrm{d}x \\ &+ \frac{\mu_2}{2}\sum_{i=1}^{n}\int_\Omega\left(v_i^k - \nabla\cdot\vec{w}_i\right)^2\mathrm{d}x\end{aligned} \quad (22)$$

$$\begin{aligned}\varepsilon_3(\vec{v}) = &\sum_{i=1}^{n}\int_\Omega[\alpha + \beta|v_i|]\delta(\varphi_i^{k+1})\mathrm{d}x \\ &+ \sum_{i=1}^{n}\int_\Omega\lambda_{2i}^k(v_i - \nabla\cdot\vec{w}_i^{k+1})\mathrm{d}x \\ &+ \frac{\mu_2}{2}\sum_{i=1}^{n}\int_\Omega(v_i - \nabla\cdot\vec{w}_i^{k+1})^2\mathrm{d}x\end{aligned} \quad (23)$$

In summary, we can present the ADMM-P approach in a pseudo-code format as follows.

Algorithm: ADMM-P for segmentation with depth

Step 1: Initialize the unknown values $c^0, \varphi^0, \vec{w}^0, v^0, \vec{\lambda}_1^0, \lambda_2^0$.

Step 2: For $k \geq 1$, solve the following problems alternatively.

2.1. Sub problem 1 about c^{k+1}:

$$c^{k+1} = Arg\min_{c}\left\{\varepsilon_0(c) = E\left(c, \varphi^k, \vec{w}^k, v^k, \vec{\lambda}_1^k, \lambda_2^k\right)\right\}.$$

2.2. Sub problem 2 about φ^{k+1}:

$$\varphi^{k+1} = Arg\min_{\varphi}\left\{\varepsilon_1(\varphi) = E\left(c^{k+1}, \varphi, \vec{w}^k, v^k, \vec{\lambda}_1^k, \lambda_2^k\right)\right\}.$$

2.3. Sub problem 3 about $\vec{w}^{k+1}$:

$$\vec{w}^{k+1} = Arg\min_{\vec{w}}\left\{\varepsilon_2(\vec{w}) = E\left(c^{k+1}, \varphi^{k+1}, \vec{w}, v^k, \vec{\lambda}_1^k, \lambda_2^k\right)\right\},$$

$$s.t. \qquad \left|\vec{w}_i^{k+1}\right| = 1,\ i = 1, 2, \ldots n.$$

2.4. Sub problem 4 about v^{k+1}:

$$v^{k+1} = Arg\min_{v}\left\{\varepsilon_3(v) = E\left(c^{k+1}, \varphi^{k+1}, \vec{w}^{k+1}, v, \vec{\lambda}_1^k, \lambda_2^k\right)\right\}.$$

2.5. Update Lagrange multiplier $\vec{\lambda}$ via (18) and (19).

Step 3: The above iterations will terminate if the stopping criteria (described in section 4) are satisfied.

Whether the above proposed ADMM method can be suitably applied for solving the non-convex and non-smooth problems in computer vision has attracted extensive attention. The authors in [39,40] discussed this issue in detail and provided many applications in which many similar algorithms have been developed and successfully used to achieve excellent performances via solving a variety of non-convex problems. In addition, many other authors [18,19,26,27,29,30] also have made a success of applying the ADMM method to different problems. In this paper, we adopt a similar research route to design a new algorithm to deal with the non-convex and non-smooth problem for the segmentation problem with depth.

Next we will consider each sub-problem in above algorithm individually.

4 Minimization of Each Sub-problem

4.1 Estimation of the Piecewise Constant Parameters

In the $(k+1)$ step of the proposed ADMM, the average image intensity values c_i in different regions can be obtained by using the standard variational method based on (14) and (20), which are given by

$$c_i^{k+1} = \frac{\int_\Omega f H(\varphi_i^k) \prod_{j=1}^{i-1} (1 - H(\varphi_j^k)) \mathrm{d}x}{\int_\Omega H(\varphi_i^k) \prod_{j=1}^{i-1} (1 - H(\varphi_j^k)) \mathrm{d}x}, \quad i = 1, 2, \ldots, n, \tag{24a}$$

$$c_{n+1}^{k+1} = \frac{\int_\Omega f \prod_{j=1}^{n}(1-H(\varphi_j^k))\mathrm{d}x}{\int_\Omega \prod_{j=1}^{n}(1-H(\varphi_j^k))\mathrm{d}x}. \tag{24b}$$

4.2 Calculation of the Level Set Functions

For the minimization sub-problems (15) and (21) with respect to the level set functions φ_i, the corresponding Euler–Lagrange equations are given by

$$\begin{cases} [\alpha+\beta|v_i^k|]\delta'(\varphi_i)+\nabla\cdot\vec{\lambda}_{1i}^k+\mu_1\nabla\cdot(\vec{w}_i^k-\nabla\varphi_i) \\ +\delta(\varphi_i)(f-c_i^{k+1})^2\prod_{j=1}^{i-1}(1-H(\varphi_j)) \\ -\delta(\varphi_i)\left[\sum_{s=i+1}^{n+1}\left\{(f-c_s^{k+1})^2H(\varphi_s)\right.\right. \\ \left.\left.\prod_{j=1}^{i-1}(1-H(\varphi_j))\prod_{j=i+1}^{s-1}(1-H(\varphi_j))\right\}\right]=0 \text{ in } \Omega \\ (\vec{\lambda}_{1i}^k+\mu_1(\vec{w}_i^k-\nabla\varphi_i))\cdot\vec{n}=0 \quad \text{on } \partial\Omega \end{cases}, \tag{25a}$$

where $\vec{w}_i^k, \vec{v}_i^k$ are fixed temporarily when φ_i^{k+1} is calculated by using the semi-implicit difference scheme and Gauss–Seidel iterative method. To be more specific, the Gauss–Seidel iterative method can be used for the linear terms of (25a) $\nabla\cdot\vec{\lambda}_{1i}^k+\mu_1\nabla\cdot(\vec{w}_i^k-\nabla\varphi_i)$, while the nonlinear terms:

$$\begin{aligned} &[\alpha+\beta|v_i^k|]\delta'(\varphi_i)+\delta(\varphi_i)\cdot(f-c_i^{k+1})^2 \\ &\prod_{j=1}^{i-1}(1-H(\varphi_j))-\delta(\varphi_i)\left[\sum_{s=i+1}^{n+1}\left\{(f-c_s^{k+1})^2H(\varphi_s)\right.\right. \\ &\left.\left.\prod_{j=1}^{i-1}(1-H(\varphi_j))\prod_{j=i+1}^{s-1}(1-H(\varphi_j))\right\}\right] \end{aligned}$$

need to be calculated by an explicit difference scheme. According to the standard technique introduced by Zhao and Chan [13], we use $|\nabla\varphi_i|$ to replace $\delta(\varphi_i)$, which facilitates accelerating the evolution process [37], and then directly utilize $|\nabla\varphi_i|=1$. The final calculation result of φ_i is shown as follows

$$\begin{aligned} \varphi_i^{k+1} = &\left\{\left(\varphi_{i(m-1,l)}^{k+1}+\varphi_{i(m,l-1)}^{k+1}+\varphi_{i(m+1,l)}^{k}+\varphi_{i(m,l+1)}^{k}\right)\right. \\ &-\nabla\cdot\vec{w}_i^k-\nabla\cdot\vec{\lambda}_{1i}^k/\mu_1 \\ &-\left(f-c_i^{k+1}\right)^2\prod_{j=1}^{i-1}\left(1-H\left(\varphi_j^k\right)\right)/\mu_1 \\ &+\sum_{s=i+1}^{n+1}\left[\left(f-c_s^{k+1}\right)^2H(\varphi_s^k)\right. \\ &\left.\left.\prod_{j=1}^{i-1}(1-H(\varphi_j^k))\prod_{j=i+1}^{s-1}(1-H(\varphi_j^k))\right]/\mu_1\right. \\ &\left.-\left[\alpha+\beta|v_i^k|\right]\delta'(\varphi_i^k)/\mu_1\right\}/4, \end{aligned} \tag{25b}$$

where $m=1,2,\ldots,M$, $l=1,2,\ldots,N$ and $M\times N$ denotes the size of the image.

4.3 Minimization of the Auxiliary Variable $\vec{w}_i$

The Euler–Lagrange equations with respect to $\vec{w}_i$ can be derived from (16) and (22) via calculus of variation when the variables φ_i^{k+1}, $\vec{v}_i^k$ are kept constant temporarily,

$$\begin{cases} \vec{\lambda}_{1i}^k+\mu_1\left(\vec{w}_i-\nabla\varphi_i^{k+1}\right)+\nabla\lambda_{2i}^k+\mu_2\left(v_i-\nabla\cdot\vec{w}_i\right)=0 \\ \text{s.t.} \quad |\vec{w}_i|=1 \end{cases}. \tag{26}$$

The first equation of (26) can be solved by using the fast Fourier transform (FFT) [30]. We now detail the FFT implementation as follows

$$\begin{aligned} &\mu_1\vec{w}_i-\mu_2\nabla\left(\nabla\cdot\vec{w}_i\right) \\ &=-\vec{\lambda}_{1i}^k-\nabla\lambda_{2i}^k+\mu_1\nabla\varphi_i^{k+1}-\mu_2\nabla v_i^k \end{aligned} \tag{27a}$$

$$\begin{cases} \mu_1 w_{i1}-\mu_2\left(\partial_{xx}w_{i1}+\partial_{xy}w_{i2}\right) \\ \quad=\mu_1\partial_x\varphi_i^{k+1}-\lambda_{1i1}^k-\partial_x\lambda_{2i}^k-\mu_2\partial_x v_i^k \\ \mu_1 w_{i2}-\mu_2\left(\partial_{yx}w_{i1}+\partial_{yy}w_{i2}\right) \\ \quad=\mu_1\partial_y\varphi_i^{k+1}-\lambda_{1i2}^k-\partial_y\lambda_{2i}^k-\mu_2\partial_y v_i^k \end{cases}. \tag{27b}$$

For clarity, we introduce $g_{i1}=\mu_1\partial_x\varphi_i^{k+1}-\lambda_{1i1}^k-\partial_x\lambda_{2i}^k-\mu_2\partial_x v_i^k$ and $g_{i2}=\mu_1\partial_y\varphi_i^{k+1}-\lambda_{1i2}^k-\partial_y\lambda_{2i}^k-\mu_2\partial_y v_i^k$. Then we can rewrite (27b) as

$$\begin{cases} \mu_1 w_{i1}-\mu_2\left(\partial_{xx}w_{i1}+\partial_{xy}w_{i2}\right)=g_{i1} \\ \mu_1 w_{i2}-\mu_2\left(\partial_{yx}w_{i1}+\partial_{yy}w_{i2}\right)=g_{i2} \end{cases}. \tag{28}$$

As in [27,29,30], after introducing the identity operator $If(m,l)=f(m,l)$ and shifting operators $S_x^{\pm}f(m,l)=f(m\pm1,l)$, $S_y^{\pm}f(m,l)=f(m,l\pm1)$, (28) can be rewritten as

$$\begin{cases} \mu_1 w_{i1}-\mu_2\left(\left(S_x^- -2I+S_x^+\right)w_{i1}\right. \\ \left.+\left(S_x^+S_y^- -S_x^+S_y^- -I+S_y^-\right)w_{i2}\right)=g_{i1} \\ \mu_1 w_{i2}-\mu_2\left(\left(S_y^+ -S_y^+S_x^- -I+S_x^-\right)w_{i1}\right. \\ \left.+\left(S_y^- -2I+S_y^+\right)w_{i2}\right)=g_{i2} \end{cases}. \tag{29}$$

Based on the discrete Fourier transform, we have the following FFT properties for the shifting operators

$$FS_x^{\pm}f\left(y_m,y_l\right)=e^{\pm\sqrt{-1}z_m}Ff\left(y_m,y_l\right), \tag{30}$$

$$FS_y^{\pm} f(y_m, y_l) = e^{\pm\sqrt{-1}Z_l} Ff(y_m, y_l), \tag{31}$$

where $f(y_m, y_l)$ is the function in time domain, y_m and y_l are discrete frequencies. Let $Z_m = \frac{2\pi}{N_1} y_m$, $y_m = 1, 2, \ldots, N_1$ and $Z_l = \frac{2\pi}{N_2} y_l$, $y_l = 1, 2, \ldots, N_2$, then (29) can be transformed into the following algebraic equations

$$\begin{pmatrix} a_{11} & a_{12} \\ a_{21} & a_{22} \end{pmatrix} \begin{pmatrix} F(w_{i1}) \\ F(w_{i2}) \end{pmatrix} = \begin{pmatrix} F(g_{i1}) \\ F(g_{i2}) \end{pmatrix}. \tag{32a}$$

where the coefficients are

$$\begin{aligned} a_{11} &= \mu_1 - 2\mu_2 (\cos Z_m - 1), \\ a_{12} &= -\mu_2 \left(1 - \cos Z_l + \sqrt{-1} \sin Z_l\right) \\ &\quad \left(-1 + \cos Z_m + \sqrt{-1} \sin Z_m\right), \\ a_{21} &= -\mu_2 \left(1 - \cos Z_m + \sqrt{-1} \sin Z_m\right) \\ &\quad \left(-1 + \cos Z_l + \sqrt{-1} \sin Z_l\right), \\ a_{22} &= \mu_1 - 2\mu_2 (\cos Z_l - 1), \end{aligned} \tag{32b}$$

The determinant of this coefficient matrix is shown as follows, and more details can be referred to [29].

$$D = \mu_1^2 - 2\mu_1\mu_2 (\cos Z_m + \cos Z_l - 2). \tag{32c}$$

This value is always positive for all discrete frequencies if $\mu_1 > 0$. Then, the discrete inverse Fourier transform can be used to update $\vec{w}_i^k$ as follows

$$\begin{cases} \tilde{w}_{i1}^{k+1} = \Re\left(F^{-1}\left(\frac{a_{22}F(g_{i1}) - a_{12}F(g_{i2})}{D}\right)\right) \\ \tilde{w}_{i2}^{k+1} = \Re\left(F^{-1}\left(\frac{-a_{21}F(g_{i1}) + a_{11}F(g_{i2})}{D}\right)\right) \end{cases}. \tag{33}$$

Finally, a simple projection technique can be used to guarantee the constraint $|\vec{w}_i| = 1$ to be satisfied if we define

$$\vec{w}_i^{k+1} = \frac{\vec{\tilde{w}}_i^{k+1}}{\left|\vec{\tilde{w}}_i^{k+1}\right|}. \tag{34}$$

4.4 Minimization of the Auxiliary Variable v_i

For the minimization problem of (17) and (23), we can derive the Euler–Lagrange equation with respect to v_i while fixing the variables φ_i^{k+1}, $\vec{w}_i^{k+1}$ temporarily,

$$\beta \frac{v_i}{|v_i|} \delta\left(\varphi_i^{k+1}\right) + \lambda_{2i}^k + \mu_2 \left(v_i - \nabla \cdot \vec{w}_i^{k+1}\right) = 0. \tag{35}$$

This equation can be solved by using the analytical soft thresholding formula [19], which is given by

$$v_i^{k+1} = Max\left(\left|\nabla \cdot \vec{w}_i^{k+1} - \frac{\lambda_{2i}^k}{\mu_2}\right| - \frac{\beta\delta\left(\varphi_i^{k+1}\right)}{\mu_2}, 0\right) \frac{\nabla \cdot \vec{w}_i^{k+1} - \frac{\lambda_{2i}^k}{\mu_2}}{\left|\nabla \cdot \vec{w}_i^{k+1} - \frac{\lambda_{2i}^k}{\mu_2}\right|}. \tag{36}$$

4.5 Updating the Lagrange Multipliers

At the end of each step, we need to update the Lagrange multipliers $\vec{\lambda}_{1i}^k$ and λ_{2i}^k after all sub-minimization problems have achieved their minimum, i.e.,

$$\vec{\lambda}_{1i}^{k+1} = \vec{\lambda}_{1i}^k + \mu_1 \left(\vec{w}_i^{k+1} - \nabla\varphi_i^{k+1}\right), \tag{37}$$

$$\lambda_{2i}^{k+1} = \lambda_{2i}^k + \mu_2 \left(v_i^{k+1} - \nabla \cdot \vec{w}_i^{k+1}\right). \tag{38}$$

In summary, all the proposed sub-problems can be solved effectively as discussed above. As in the alternating process, each sub-problem is easy to solve as other variables are kept as constants. As to the stopping criteria for each sub-problem, we will discuss them in next section.

5 Numerical Experiments

In this section, some numerical experiments on synthetic, and real images are presented to validate the performance and efficiency of proposed model and algorithm. All experiments are implemented using Matlab7.8 on a PC (Intel (R), CPU 2.60GHz). The proposed ADMM-P method will be compared with a traditional GDM [12]. For the purpose of fair comparison, the same initialization for both methods is used.

As described in [30], the iterations need to be terminated when the following criteria are satisfied:

(I) We need to monitor the following constraint errors in iterations:

$$\begin{aligned} \left(R_{\vec{w}i}^k \; R_{vi}^k\right) = \Big(&\left\|\vec{w}_i^k - \nabla\varphi_i^k\right\|_{L^1} / \left\|\vec{w}_i^0 - \nabla\varphi_i^0\right\|_{L^1} \\ &\left\|v_i^k - \nabla \cdot \vec{w}_i^k\right\|_{L^1} / \left\|v_i^0 - \nabla \cdot \vec{w}_i^0\right\|_{L^1}\Big), \end{aligned} \tag{39}$$

where, $\|\cdot\|_{L^1}$ denotes the L^1 norm on image domain Ω. All components in (39) are calculated point by point. If $R_i^k < \varepsilon$(ε is a small enough parameter) for $i = 1, 2, \ldots, n$, the overall iteration will be stopped. These good numerical indicators are also used to determinate the values of $\mu_i (i = 1, 2)$, which is the basis of penalty parameter adjustment.

(II) During iteration, the relative errors of Lagrange multipliers and the solution φ_i^k should be monitored. They should decrease to a sufficiently small level:

$$\left(R^k_{\vec{\lambda}1i} \quad R^k_{\lambda 2i}\right) = \left(\left\|\vec{\lambda}^k_{1i} - \vec{\lambda}^{k-1}_{1i}\right\|_{L^1} / \left\|\vec{\lambda}^{k-1}_{1i}\right\|_{L^1} \right.$$
$$\left. \left\|\lambda^k_{2i} - \lambda^{k-1}_{2i}\right\|_{L^1} / \left\|\lambda^{k-1}_{2i}\right\|_{L^1}\right), \tag{40}$$

$$R^k_{\varphi i} = \left\|\varphi^k_i - \varphi^{k-1}_i\right\|_{L^1} / \left\|\varphi^{k-1}_i\right\|_{L^1}. \tag{41}$$

Note that (40) can be quite small if the penalty parameters are large. This is due to the explicit dependency on the penalty parameters.

(III) The relative energy error can be chosen as stopping criterion:

$$R^k_e = \left|E^{k+1} - E^k\right| / |E^k|. \tag{42}$$

where E^k is the energy value of (13a). The computation stops automatically when R^k_e is less than a predefined tolerance, which indicates that the energy approaches its steady state.

Until now, the presentation of the proposed ADMM-P is complete and we will show its effectiveness in next subsection with extensive experiments. Just keep in mind that all numerical quantities are plotted in log scale.

Next, we introduce some specific methods to tune parameters in the process of implementing the proposed approach. The two parameters in the NMS functional (1), α and β, control the length and curvature of the segmentation boundary. The ratio between α and β is in relation to the connectivity and smoothness of the level lines. As discussed in [30], the connection of disconnected level lines and smoothness of level lines can be guaranteed by a larger parameter β. In addition, another two parameters associated with Lagrange multipliers are in the augmented Lagrange energy functional (13): μ_1 and μ_2, and they can be determined according to relative residuals (39), relative errors of the Lagrange multiplier (40), relative errors of φ^k_i (41) and the energy curve. One example is given to show such selection in Experiment 5.1.

5.1 Experiment on a Synthetic Image (Two Objects and One Background)

The first testing image is a synthetic image containing a bar and a U-sharp object (size 128×128) as shown in Fig. 1a. In this example, two level set functions are required to describe the shapes. In order to speed up the evolution of contours, we initialize the two level set functions in Fig. 1b using the results from the piecewise constant image segmentation by using variational level set method. The final results of segmentation with depth are presented in Fig. 1c.

In this experiment, the required parameters are selected as $\alpha = 0.5, \beta = 3, \mu_1 = 3000, \mu_2 = 3, \varepsilon = 3$, respectively, for the proposed ADMM-P algorithm. In order to determine the ordering relations of the bar and the U-shape object, we minimize the energy functional based on the assumptions that the U-shape object is occluded by the bar or the bar is occluded by the U-shape object. The results are listed in Table 1, from which we can deduce that the bar, the U-shape object and the background are ordered from the nearest to farthest with respect to the observer.

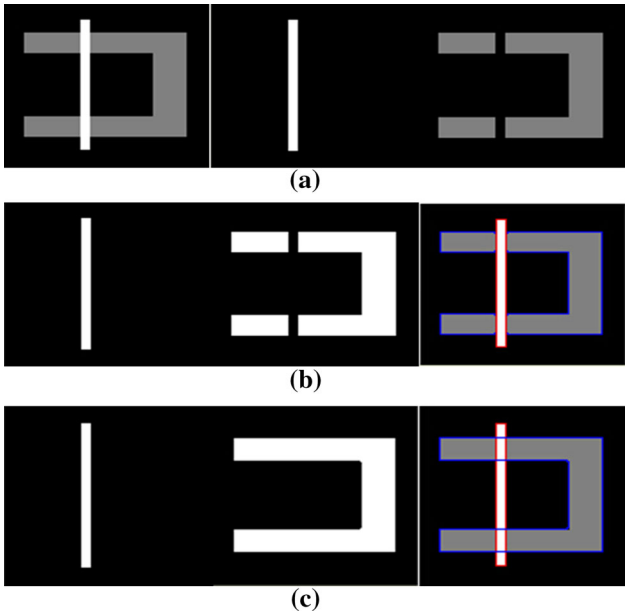

Fig. 1 Segmentation with depth for a bar and a U-sharp object. **a** The original image and the results using traditional piecewise constant image segmentation model; **b** initialization for segmentation with depth; **c** segmentation results using both GDM and ADMM-P method

Table 1 Minimal energies of different ordering relations

Possible order	Minimum of energy functional
Bar → U rod	19.81
U rod → Bar	21.34

As to the case that the U-shape object is occluded by the bar, we illustrate the relative residuals (39), relative errors of the Lagrange multipliers (40), relative errors of φ^k_i (41) and energy curve in Fig. 2. The graphs come from Fig. 1c. From these plots, one can observe that the proposed algorithm has converged before 30 iterations. They also give an important clue about how to choose penalty parameters $\mu_i (i = 1, 2)$. In order to guarantee convergence as well as the speed of convergence, the constraint errors $R^k_{\vec{w}i}, R^k_{vi}, R^k_{\vec{\lambda}1i}, R^k_{\lambda 2i}$ should converge steadily with nearly the same speed. If $R^k_{\vec{w}i}, R^k_{vi}$ go to zero faster than others, then one can decrease μ_i and vice versa. $R^k_{\vec{w}i}, R^k_{vi}$ will converge to zero with the same speed as the iteration proceeds and the energy will decrease to a steady constant value when μ_i are chosen properly.

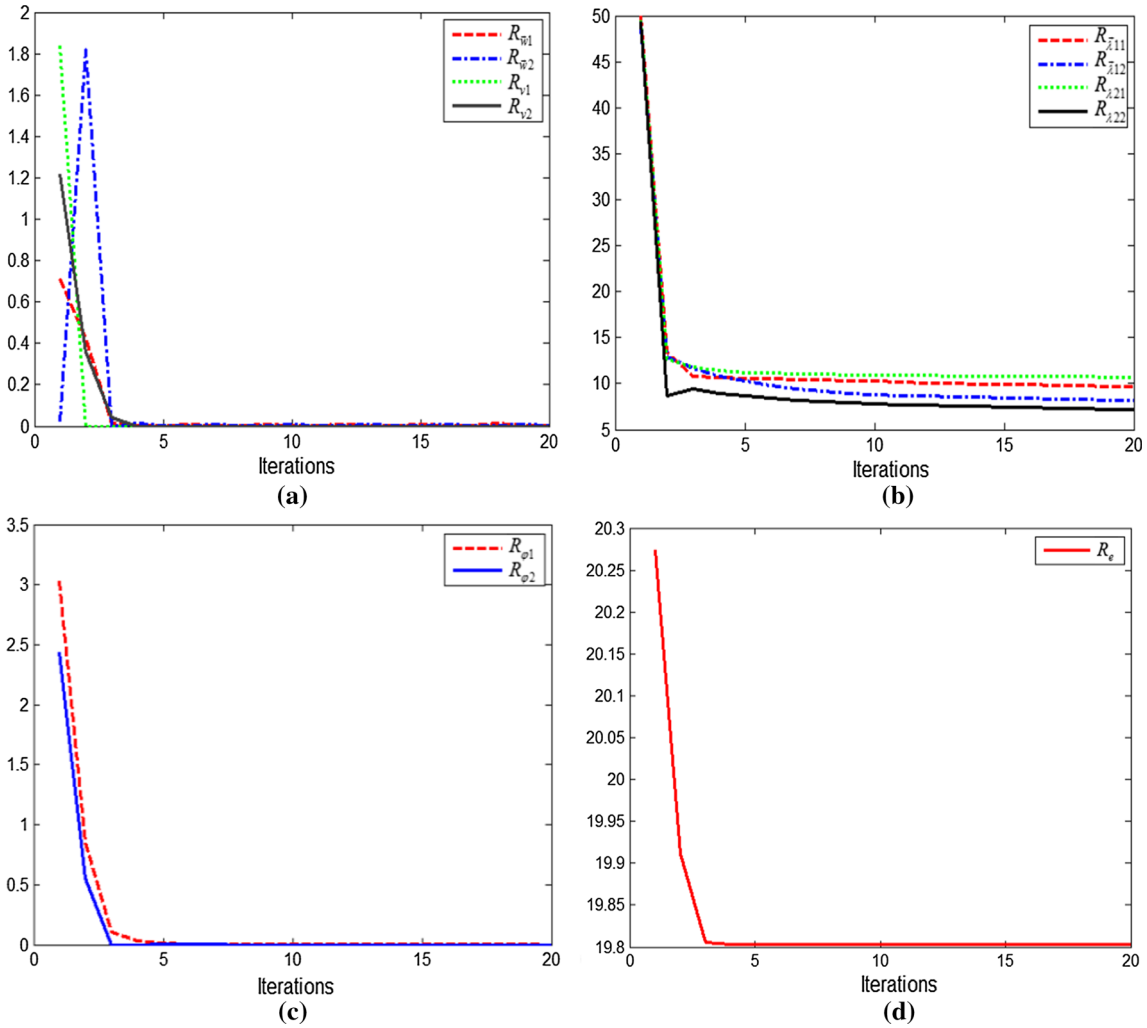

Fig. 2 The relative residual plots of **a** auxiliary variables; **b** Lagrange multipliers; **c** level set functions; **d** the energy functional

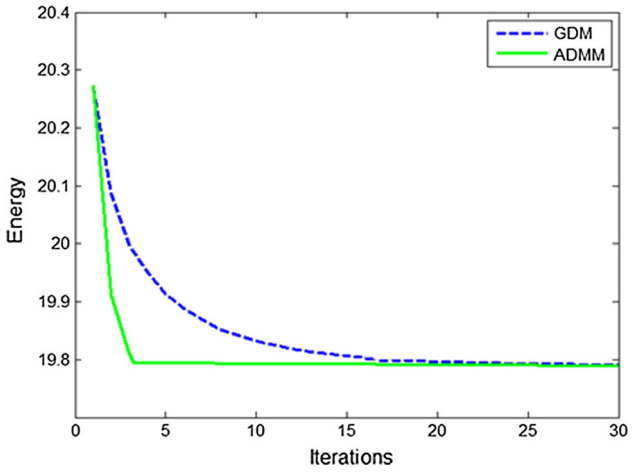

Fig. 3 Plots of decaying energy by GDM and ADMM-P methods

Table 2 Number of iterations and time costs using GDM and ADMM-P methods

Approaches	Iterations	Time (s)
Figure 1c: GDM	23	1.74
Figure 1c: ADMM-P	4	0.21

As to efficiency of the proposed algorithm, the energy curves produced by using the GDM [12] and the proposed ADMM-P are shown in Fig. 3 and the time costs are shown in Table 2. It is easy to see that the ADMM-P has faster convergence rate and higher efficiency. The parameters for the GDM method in this experiment are set as $\alpha = 0.5, \beta = 3, \lambda = 0.5, \varepsilon = 3, \mathrm{d}t = 5 \times 10^{-4}$. By considering the comparisons of these two algorithms, we plot the energy functional of the original NMS model.

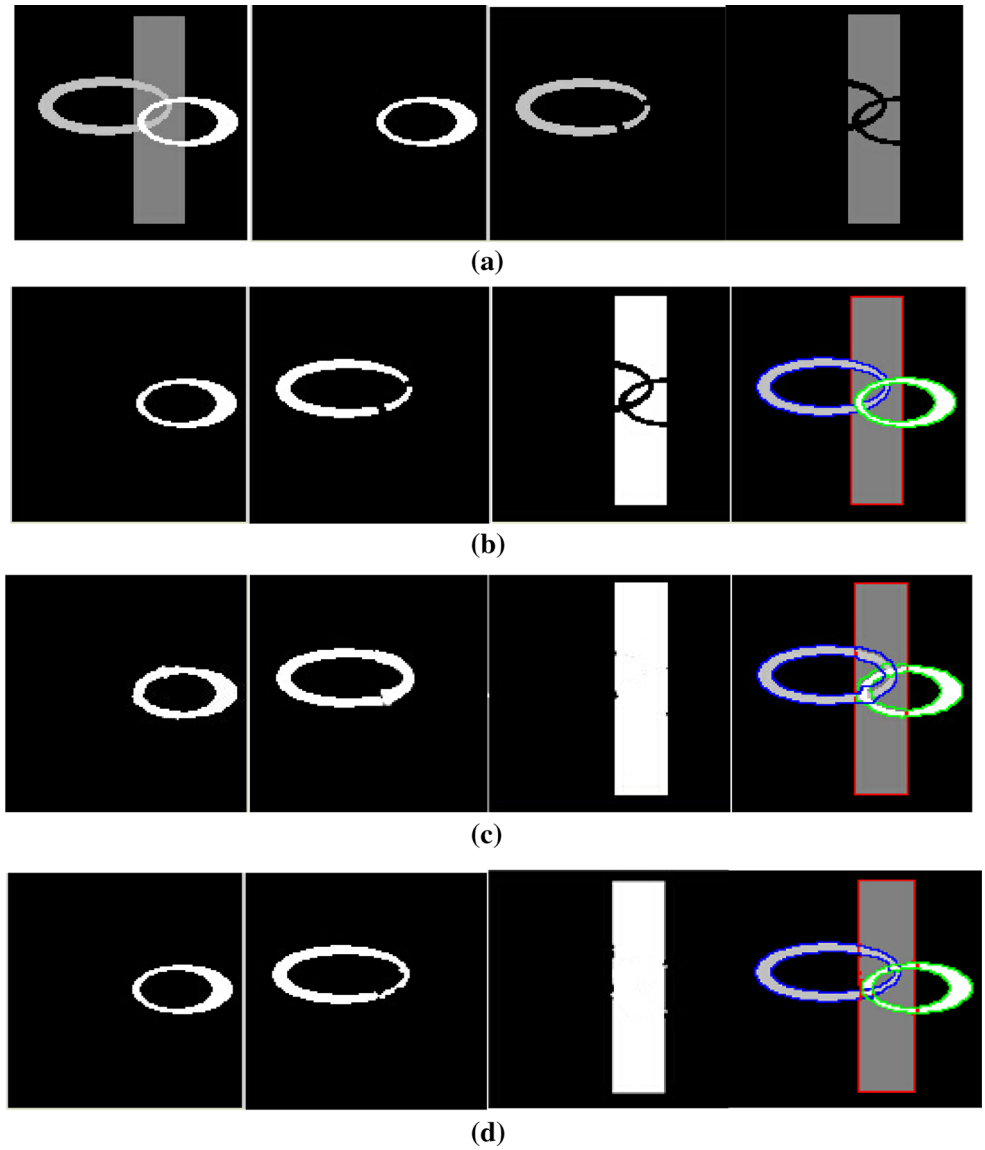

Fig. 4 Segmentation with depth for an image with one bar and two circles. **a** The original image and three regions via traditional image segmentation model; **b** the initializations for segmentation with depth; **c** the results via GDM; **d** the results via ADMM-P

Table 3 Minimal energies of different ordering relations

Possible Order	Minimum of energy functional
Small circle → Big circle → Bar	20.17
Small circle → Bar → Big circle	21.56
Big circle → Small circle → Bar	25.81
Big circle → Bar → Small circle	26.49
Bar → Small circle → Big circle	26.74
Bar → Big circle → Small circle	26.72

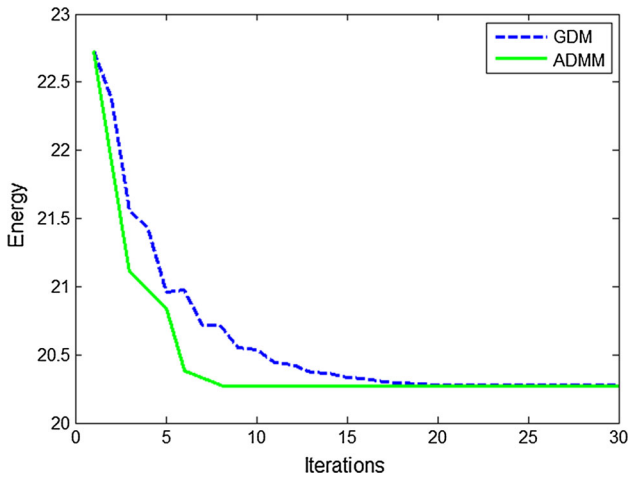

Fig. 5 Comparison of energy curves obtained by GDM and ADMM-P

Table 4 Number of iterations and time costs using GDM and ADMM-P

Approaches	Iterations	Time (sec)
Figure 4c: GDM	19	1.29
Figure 4d: ADMM-P	8	0.48

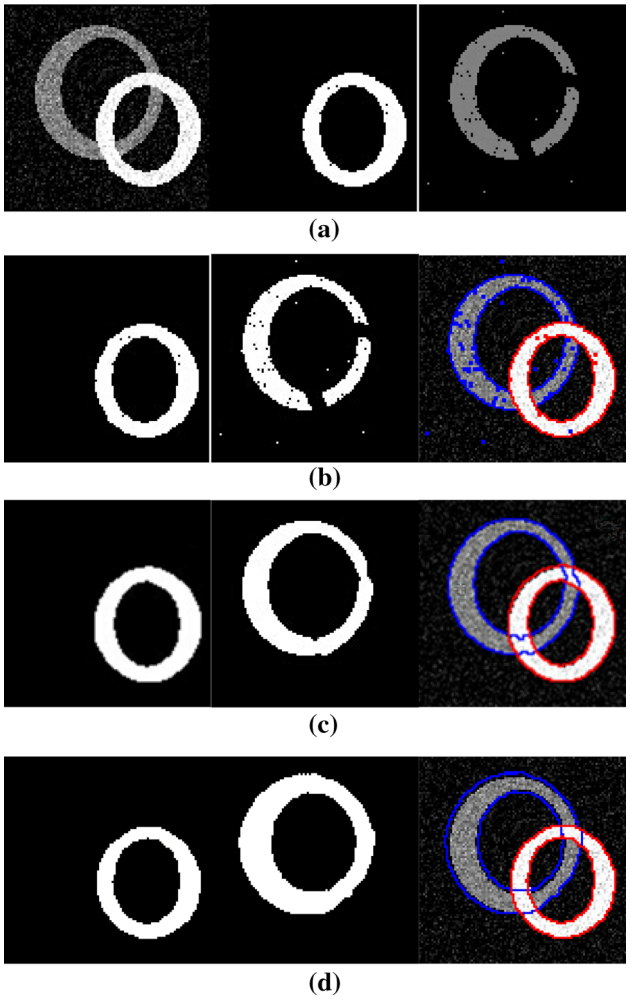

Fig. 6 Segmentation with depth of a noise image. **a** The original image and the segmentation results via traditional image segmentation model; **b** the initializations for segmentation with depth; **c** the results of GDM; **d** final results of ADMM-P

5.2 Experiment on synthetic image (Three Objects and a Background)

The second testing image is a synthetic one with two circles and a bar (size 128 × 128) shown in Fig. 4a. There are totally four regions to be segmented including three objects and a background. In this case, three level set functions are required. In Fig. 4b, the results by piecewise constant segmentation method are used as the initialization for the level set functions. The final results obtained by the GDM and ADMM-P are presented in Fig. 4c, d, respectively.

Table 5 Minimal energies of different ordering relations

Possible order	Minimum of energy functional
White circle → Gray circle	17.33
Gray circle → White circle	19.25

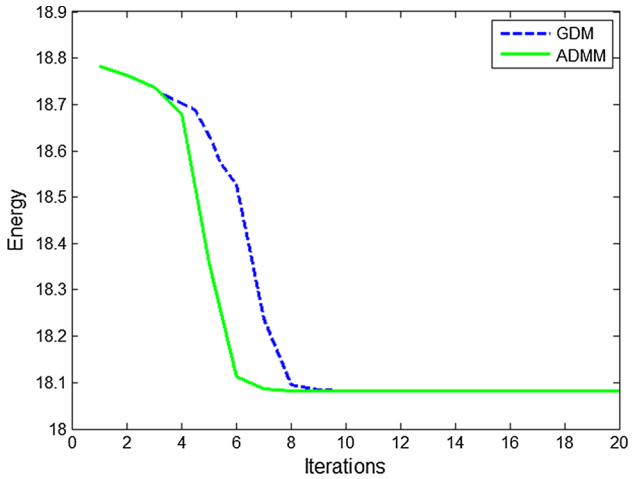

Fig. 7 Comparison of energy curves obtained by GDM and ADMM-P

Table 6 Number of iterations and cost time using GDM and ADMM-P

Approaches	Iterations	Time (s)
Figure 6c: GDM	14	0.85
Figure 6d: ADMM-P	11	0.46

The parameters used in the proposed ADMM-P method are chosen as $\alpha = 0.3$, $\beta = 2$, μ_1=600, μ_2=3, $\varepsilon = 5$. In this experiment, there are $3! = 6$ possible combinations shown in Table 3 to be considered. After minimizing the energy functional based on the six assumptions separately, the ordering relations between the small circle, the big circle and the bar can be determined. From Table 3, we know that the correct ordering from the nearest to the most further is: small circle, big circle, bar and the background.

In the case of correct ordering, we present the plots of energy decay and time costs in Fig. 5 and Table 4, respectively, by using the GDM and ADMM-P methods in order to compare their computational efficiency. The parameters for the GDM method in this experiment are $\alpha = 0.3$, $\beta = 2$, λ= 0.1, $\varepsilon = 3$, $dt = 1 \times 10^{-4}$.

5.3 Experiment on a Noise Image (Two Objects and a Background)

The third experiment is conducted on a noise image (size 100 × 100) with two circles (two objects and a background)

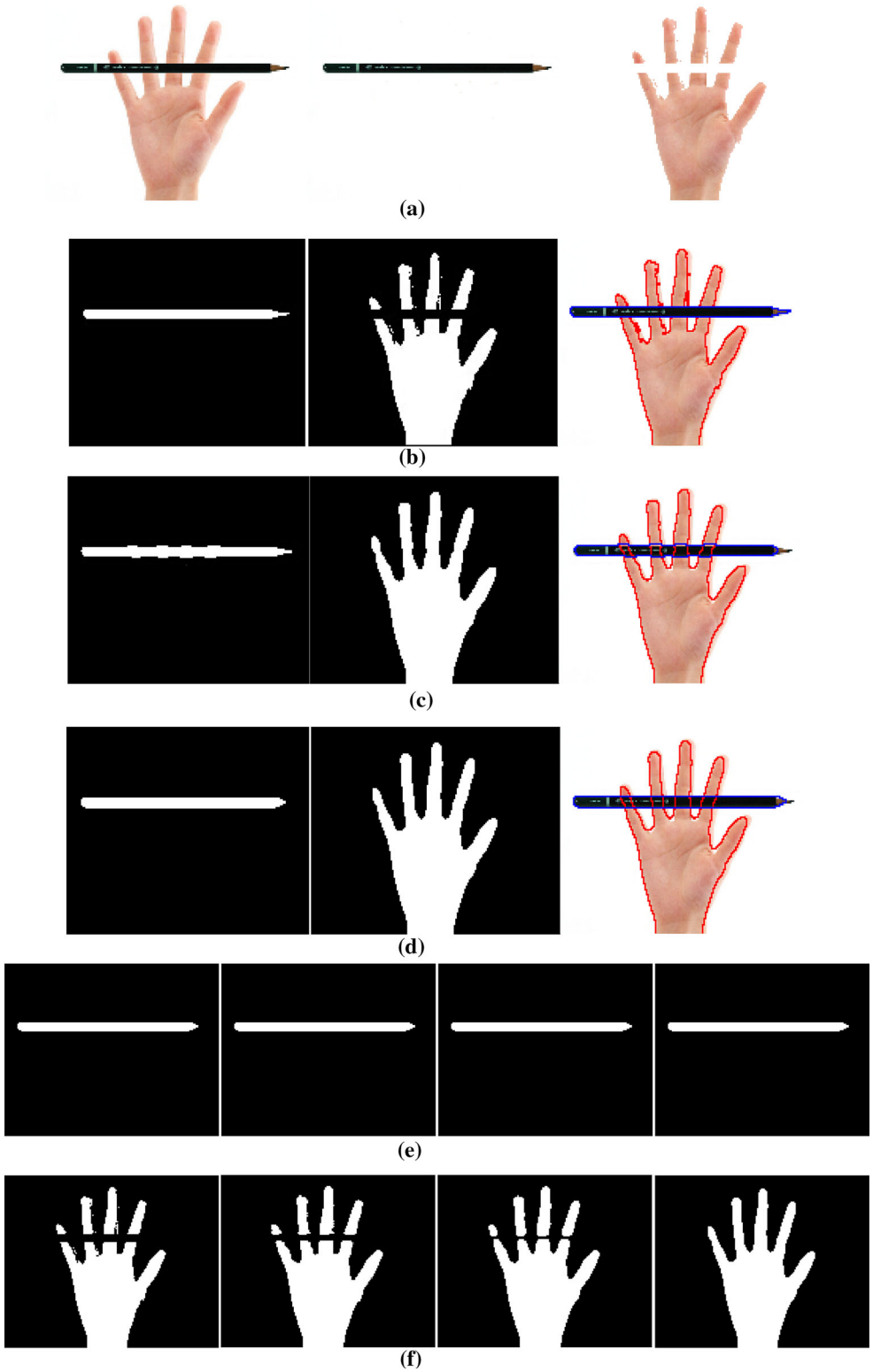

Fig. 8 Segmentation with depth for a color image with a pencil and a hand. **a** The original image and two regions via traditional image segmentation model; **b** the initializations; **c** the results via GDM; **d** final segmentation results using ADMM-P; **e** evolution process of pencil; **f** evolution process of hand

Table 7 Minimal energies of different ordering relations

Possible Order	Minimum of energy functional
Pencil → Hand	35.24
Hand → Pencil	38.56

as shown in Fig. 6a. The image is corrupted by Gaussian white noise with standard deviation 0.01. Figure 6b presents the initialization of the level set functions by using the results of piecewise constant segmentation method. The final results obtained by the GDM and ADMM-P are presented in Fig. 6c through Fig. 6d, respectively. It can be observed that the segmentation with depth is robust to noises.

In this experiment, the required parameters are selected as follows: $\alpha = 3, \beta = 2, \mu_1 = 4, \mu_2 = 3, \varepsilon = 3$ for the proposed ADMM-P method. For the ordering relations between the white circle and the gray circle, we minimize the energy functional based on the assumptions that the white circle occludes the gray circle and the gray circle occludes the white circle, respectively. From the results listed in Table 5, we can deduce that the correct ordering from the nearest to the farthest is: white circle, gray circle and the background.

In the case that white circle occludes gray circle, we further present the energy decaying trends and time costs in Fig. 7 and Table 6, respectively, obtained by using the GDM and ADMM-P methods in order to compare their computational efficiency. The parameters for the GDM method in this experiment are chosen as $\alpha = 3, \beta = 2, \lambda = 0.05, \varepsilon = 3, \mathrm{d}t = 5 \times 10^{-4}$.

5.4 Experiment on a Color Image (Two Objects and a Background)

In the last experiment, a color image with a pencil and a hand (size 256 × 242) shown in Fig. 8a is used. There is a pencil and a hand in this image, so two level set functions are required to represent the shapes. Figure 8b gives the initialization for the level set functions, and it is obtained by piecewise constant segmentation method. The final results obtained by the GDM and ADMM-P are presented in Fig. 8c, d, respectively. Figure 8e, f shows the process of evolution in details. It can be seen clearly that the pencil in the front keeps stable while fingers of the hand gradually connect behind the pencil. According to the segmentation model for vector-valued images proposed in [38], the averages of the data terms over all channels are used for coupling. In fact, the model used to solve color image segmentation with depth information can be stated as follows:

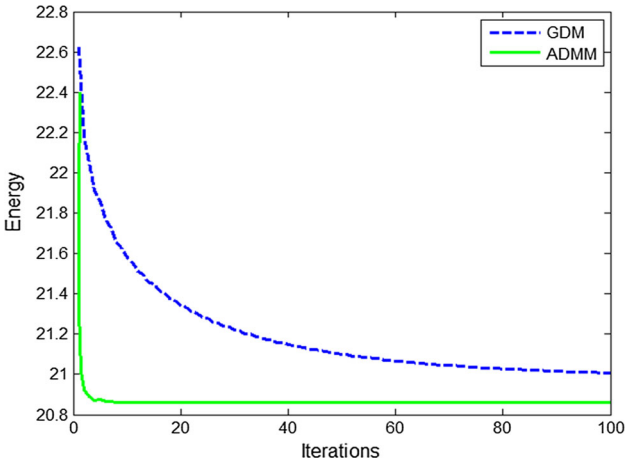

Fig. 9 Comparison of energy decreasing curves obtained by GDM and ADMM-P

Table 8 Number of iterations and time costs using GDM and ADMM-P

Approaches	Iterations	Time (s)
Figure 8c: GDM	86	4.63
Figure 8d: ADMM-P	29	1.75

$$E = \sum_{i=1}^{n} \int_{\Omega} [\alpha + \beta \, |\nabla \cdot (\nabla \varphi_i)|] \delta(\varphi_i) \, \mathrm{d}x + \sum_{l=1}^{m} \left\{ \sum_{i=1}^{n} \int_{\Omega} (f_l - c_{il})^2 H(\varphi_i) \prod_{j=1}^{i-1} \big(1 - H(\varphi_j)\big) \mathrm{d}x \right\} + \sum_{l=1}^{m} \int_{\Omega} \big(f_l - c_{(n+1)l}\big)^2 \prod_{j=1}^{n} \big(1 - H(\varphi_j)\big) \mathrm{d}x \tag{43a}$$

$$\text{s.t.} \quad |\nabla \varphi_i| = 1 \tag{43b}$$

where $l = 1, 2, \ldots, m$ denotes the number of layers of a vector-valued image.

In this experiment, the parameters for the ADMM-P are selected as: $\alpha = 0.5, \beta = 10, \mu_1 = 85, \mu_2 = 3, \varepsilon = 3$. In order to determine the ordering relations of the pencil and the hand, we minimize the energy functional based on the assumptions that the pencil occludes the hand, or the hand occludes the pencil, respectively. From the results listed in Table 7, we can choose the correct ordering from the nearest to the farthest is: pencil, hand and the background.

In the case that the pencil occludes the hand, we compare the computational efficiency between the GDM and ADMM-P methods based on their energy decaying plots in Fig. 9 and the time costs in Table 8. The parameters for the GDM method in this experiment are $\alpha = 2, \beta = 15, \lambda = 0.1, \varepsilon = 3, dt = 8 \times 10^{-5}$.

6 Conclusions

As it is known that the Nitzberg–Mumford–Shiota (NMS) model for image segmentation with depth can be described as the classical Mumford–Shah model, this model is computational expensive and time consuming. In order to solve this problem efficiently, for the variational level set formulation of the NMS, we first propose its equivalent simplified variational level set formulation by taking advantage of the property of level set functions as signed distance functions, then we develop the fast ADMM (alternating direction method of multipliers) projection method by combining the ADMM method and projection method. Thus, the original complicated problem is decomposed into a series of simple sub-problems of optimization, and each sub-problem can be easily solved accordingly. Extensive experiments have validated the effectiveness of the proposed ADMM-P approach as the ADMM-P method is much faster than the traditional algorithms based on the GDM and this may be due to the merits of the Gauss–Seidel method, soft thresholding formulas, FFT method, projection method as well as model reduction. Also, the strategies of model simplification and constraint projection can be easily extended to other variational level set models with/without curvatures.

In this paper, the number of objects in an image is known and in future, we will investigate this problem without this assumption.

Acknowledgements The work has been partially supported by the National Natural Science Foundation of China with Grant numbers 61305045, 61170106, 61363066 and 61303079.

References

1. Nitzberg, M., Mumford, D.: The 2.1D sketch. In: Proceedings of the Third IEEE International Conference on Computer Vision, pp. 138–144 (1990)
2. Yu, C.-C., Liu, Y.-J., Wu, M.T., Li, K.-Y., Fu, X.: A global energy optimization framework for 2.1D sketch extraction from monocular images. Graph. Models **76**(5), 507–521 (2014)
3. Amer, M.R., Yousefi, S., Raich, R., Todorovic, S.: Monocular extraction of 2.1D sketch using constrained convex optimization. Int. J. Comput. Vis. **112**(1), 23 (2015)
4. Zhu, W., Chan, T.F.: A variational model for capturing illusory contours using curvature. J. Math. Imaging Vis. **27**(1), 29–40 (2007)
5. Kang, S.-H., Zhu, W., Shen, J(.J.-H).: Illusory shapes via corner fusion. SIAM J. Imaging Sci. **7**(4), 1907–1936 (2014)
6. Nitzberg, M., Mumford, D., Shiota, T.: Filtering, Segmentation, and Depth. Lecture Notes in Computer Sciences, vol. 662. Springer-Verlag, Berlin (1993)
7. Mumford, D., Shah, J.: Optimal approximations by piecewise smooth functions and associated variational problems. Commun. Pure Appl. Math. **42**(5), 577–685 (1989)
8. Mumford, D.: Elastica and computer vision. In: Bajaj, C.L. (ed.) Algebraic Geometry and Its Applications, pp. 491–506. Springer-Verlag, New York (1994)
9. Esedoglu, S., March, R.: Segmentation with depth but without detecting junctions. J. Math. Imaging Vis. **18**(1), 7–15 (2003)
10. Ambrosio, L.A., Tortorelli, V.M.: Approximation of functionals depending on jumps by elliptic functionals via Γ-convegence. Commun. Pure Appl. Math. **43**(8), 999–1036 (1990)
11. Loreti, P., March, R.: Propagation of fronts in a nonlinear fourth order equation. Eur. J. Appl. Math. **2**, 203–213 (2000)
12. Zhu, W., Chan, T.F., Esedoglu, S.: Segmentation with depth: a level set approach. SIAM J. Sci. Comput. **28**(5), 1957–1973 (2006)
13. Zhao, H.-K., Chan, T.F., Merriman, B., Osher, S.: A variational level set approach to multiphase motion. J. Comput. Phys. **127**(1), 179–195 (1996)
14. Chan, T.F., Vese, L.A.: Active contours without edges. IEEE Trans. Image Process. **10**(2), 266–277 (2001)
15. Vese, L.A., Chan, T.F.: A multiphase level set framework for image segmentation using the Mumford and Shah model. Int. J. Comput. Vis. **50**(3), 271–293 (2002)
16. Osher, S., Sethian, J.A.: Fronts propagating with curvature-dependent speed: Algorithms based on Hamilton–Jacobi formulations. J. Comput. Phys. **79**(1), 12–49 (1988)
17. Smereka, P.: Semi-implicit level set methods for curvature and surface diffusion motion. J. Sci. Comput. **19**(1–3), 439–456 (2003)
18. Zhu, W., Tai, X.-C., Chan, T.F.: Image segmentation using Euler's elastica as the regularization. J. Sci. Comput. **57**(2), 414–438 (2013)
19. Wu, C., Tai, X.-C.: Augmented Lagrangian method, dual methods, and split Bregman iteration for ROF, vectorial TV, and high order models. SIAM J. Imaging Sci. **3**(3), 300–339 (2010)
20. Goldstein, T., O'Donoghue, B., Setzer, S., Baraniuk, R.: Fast alternating direction optimization methods. SIAM J. Imaging Sci. **7**(3), 1588–1623 (2014)
21. Chan, T.F., Esedoglu, S., Nikolova, M.: Algorithms for finding global minimizers of denoising and segmentation models. SIAM J. Appl. Math. **66**(5), 1632–1648 (2006)
22. Lie, J., Lysaker, M., Tai, X.-C.: A binary level set model and some applications to Mumford–Shah image segmentation. IEEE Trans. Image Process. **15**(5), 1171–1181 (2006)
23. Chan, T.F., Kang, S.-H., Shen, J(.J.-H).: Euler's elastica and curvature-based inpainting. SIAM J. Appl. Math. **63**(2), 564–592 (2002)
24. Masnou, S.: Disocclusion: a variational approach using level lines. IEEE Trans. Image Process. **11**(2), 68–76 (2002)
25. Zhu, W., Chan, T.F.: Image denoising using mean curvature of image surface. SIAM J. Imaging Sci. **5**(1), 1–32 (2012)
26. Yip, A., Zhu, W.: A fast modified Newton's method for curvature based denoising of 1D signals. Inverse Probl. Imaging **7**(3), 1075–1097 (2013)
27. Zhu, W., Tai, X.-C., Chan, T.F.: Augmented Lagrangian method for a mean curvature based image denoising model. Inverse Probl. Imaging **7**(4), 1409–1432 (2013)
28. Myllykoski, M., Glowinski, R., Karkkainen, T., Rossi, T.: A new augmented Lagrangian approach for L1-mean curvature image denoising. SIAM J. Imaging Sci. **8**(1), 95–125 (2015)
29. Tai, X.-C., Hahn, J., Chung, G.J.: A fast algorithm for Euler's elastica model using augmented Lagrangian method. SIAM J. Imaging Sci. **4**(1), 313–344 (2011)
30. Tai, X.-C.: Fast Numerical Schemes Related to Curvature Minimization: A Brief and Elementary Review, UCLA CAM Report14-40 (May, 2014)
31. Osher, S., Fedkiw, R.: Level Set Methods and Dynamic Implicit Surfaces. Springer, Berlin (2003)
32. Zhao, H.-K.: Fast sweeping method for eikonal equations. Math. Comput. **74**, 603–627 (2005)
33. Li, C., Xu, C., Gui, C., Fox, M. D.: Level set evolution without re-initialization: a new variational formulation. In: IEEE Computer

Society Conference on Computer Vision and Pattern Recognition, CVPR 2005, vol. 1, pp. 430–436, June 20 (2005)
34. Liu, C., Dong, F., Zhu, S., Kong, D., Liu, K.: New variational formulations for level set evolution without re-initialization with applications to image segmentation. J. Math. Imaging Vis. **41**(3), 194–209 (2011)
35. Duan, J., Pan, Z., Yin, X., Wei, W., Wang, G. (2014) Some fast projection methods based on Chan–Vese model for image segmentation. EURASIP J. Image Video Process. 10.1186/1687-5281-2014-7
36. Yashtini, M.: Alternating Direction Method of Multiplier for Euler's Elastica-Based Denoising, Scale Space and Variational Methods in Computer Vision, pp. 690–701. Springer, Berlin (2015)
37. Marquina, A., Osher, S.: Explicit algorithms for a new time dependent model based on level set motion for nonlinear deblurring and noise removal. SIAM J. Sci. Comput. **22**(2), 387–405 (2000)
38. Chan, T.F., Sandberg, B.Y., Vese, L.A.: Active contours without edges for vector-valued images. J. Vis. Commun. Image Represent. **11**(2), 130–141 (1970)
39. Wang, Y., Yin, W., Zeng, J.: Global convergence of ADMM in nonconvex nonsmooth optimization. arXiv preprint arXiv:1511.06324, (2015)
40. Glowinski, R., Pan, T.W., Tai, X.C.: Some facts about operator splitting and alternating direction methods. UCLA CAM Report: 16-10 (2016)

Lu Tan received the B.Sc. degree in Electronic Information Engineering in 2010 and M.Sc. degree in Computer Science and Technology in 2016 both from Qingdao University, P. R. China. She will join Curtin University in Australia as a Ph.D. candidate. Her current research interests include variational image restoration and segmentation, illusory contour capture, intelligent video analysis and 3-D medical image processing.

Zhenkuan Pan was born in 1966 in Shandong province, P. R. China. He received his Ph.D. degree in Engineering Mechanics from Shanghai Jiao Tong University, Shanghai, P. R. China in 1992. He is a Professor in College of Computer Science and Technology at Qingdao University, P. R. China. His current research interests include dynamics and optimization of multibody systems, medical simulation, and image processing.

Wanquan Liu received the B.Sc. degree in Applied Mathematics from Qufu Normal University, P. R. China, in 1985, the M.Sc. degree in Control Theory and Operation Research from Chinese Academy of Science in 1988, and the Ph.D. degree in Electrical Engineering from Shanghai Jiaotong University, in 1993. He once held the ARC Fellowship, U2000 Fellowship and JSPS Fellowship and attracted research funds from different resources over 2.4 million dollars. He is currently an Associate Professor in the Department of Computing at Curtin University and is in editorial board for nine international journals. His current research interests include large-scale pattern recognition, signal processing, machine learning and control systems.

Jinming Duan received B.Sc. (2011) in Information Science and Technology from Nanjing University of Information Science and Technology, P. R. China, and M.Sc. (2014) from Qingdao University, P. R. China. He is currently pursuing a Ph.D. in Computer Science in the University of Nottingham, UK. His research interests include variational image restoration, multiphase image segmentation, implicit surface reconstruction, medical image analysis.

Weibo Wei was born in 1981 in Shandong province, China. He received his Ph.D. degree from Nanjing University of Science and Technology in 2006. He is an Associate Professor in College of Computer Science and Technology at Qingdao University, P. R. China. His current research interests include image processing, biometric identification, automatic target recognition and tracking.

Guodong Wang was born in Weifang City, Shandong Province, P. R. China, in February, 1980. Now he is an Associate Professor in College of Computer Science and Technology, Qingdao University. He received Bachelor degree in 2001 and Master degree in 2004 in control theory and control engineer, in Qingdao University of Science and Technology, and received Ph.D. degree in pattern recognition and intelligent system in Huazhong University of Science and Technology in 2008. His research Interests include: variational image science, face recognition, intelligent video surveillance, 3D reconstruction and medical image processing and analysis.